Electronic Supplementary Material (ESI) for Nanoscale.

Supplementary Information

Fabrication of three-dimensional ordered macroporous spinel $CoFe_2O_4$ as efficient bifunctional catalysts for a positive electrode of lithium-oxygen batteries

By *Jong Guk Kim,[a†] Yuseong Noh,[b†] Youngmin Kim,[c] Seonhwa Lee,[d] and Won Bae Kim*[b]*

[a]School of Materials Science and Engineering, Gwangju Institute of Science and Technology (GIST), 261 Cheomdan-gwagiro, Buk-gu, Gwangju 500-712, South Korea

[b]Department of Chemical Engineering, Pohang University of Science and Technology (POSTECH), 77 Cheongam-Ro, Nam-gu, Pohang, Gyeongbuk 37673, South Korea

[c]Carbon Resources Institute, Korea Research Institute of Chemical Technology (KRICT), 141 Gajeong-ro, Yuseong-gu, Daejeon 34114, South Korea

[d]Department of Physics and Photon Science, Gwangju Institute of Science and Technology (GIST), 261 Cheomdan-gwagiro, Buk-gu, Gwangju 500-712, South Korea

[†] These two authors contributed equally to this work

* Corresponding Author: Tel: +82-54-279-2397. Fax: +82-54-279-5528,

E-mail: kimwb@postech.ac.kr

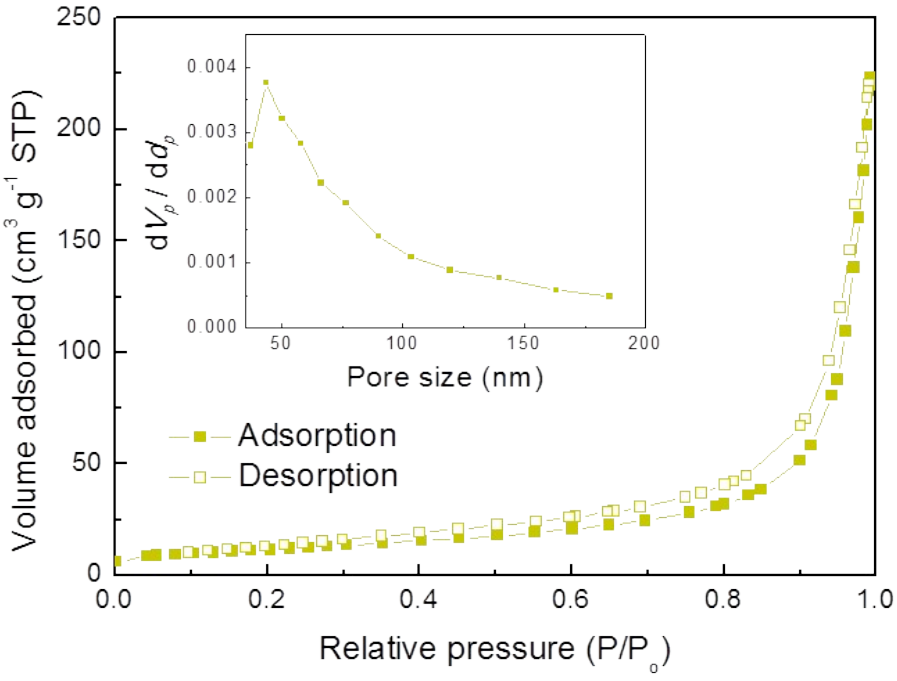

Fig. S1 Nitrogen adsorption isotherms of 3DOM CFO@60. Inset shows pore size distribution of 3DOM CFO@60.

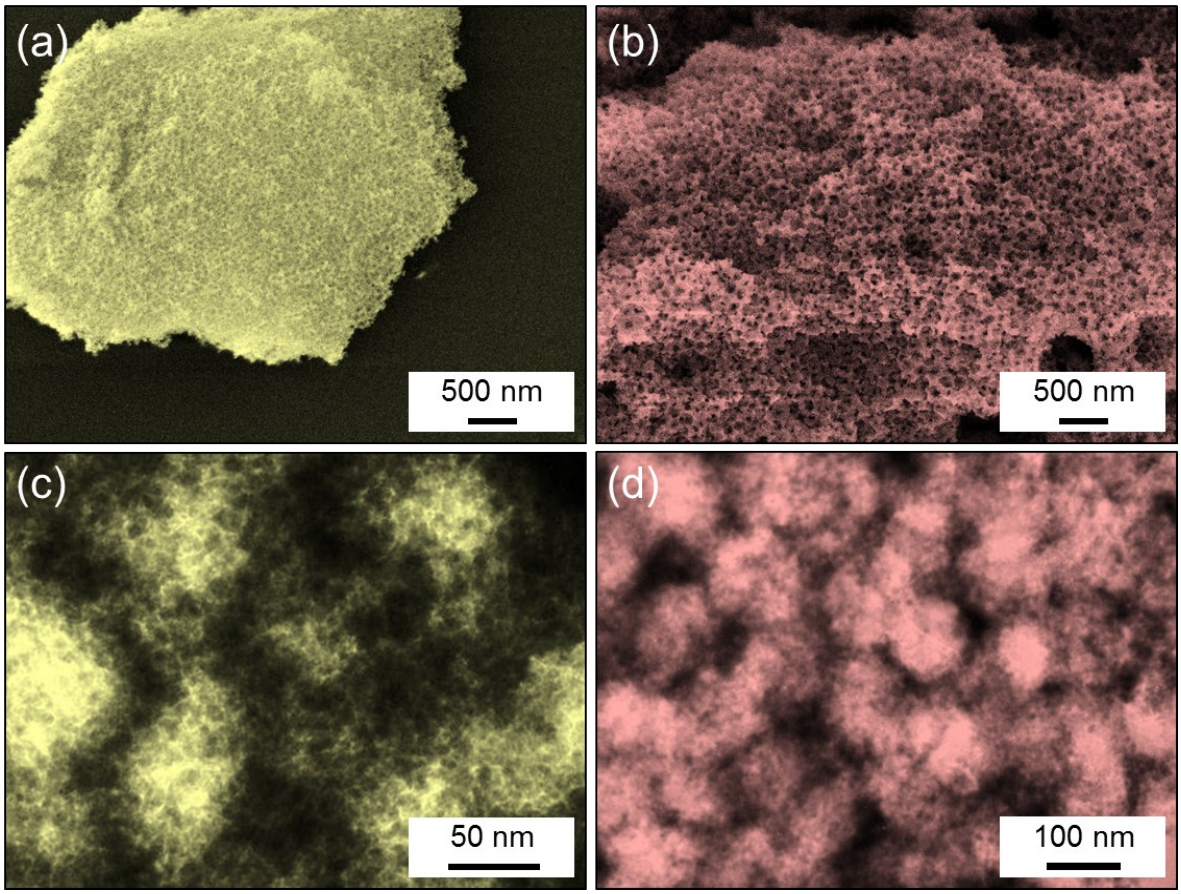

Fig. S2 SEM images (a and b) of CFO@60 and CFO@140. TEM images (c and d) of CFO@60 and CFO@140.

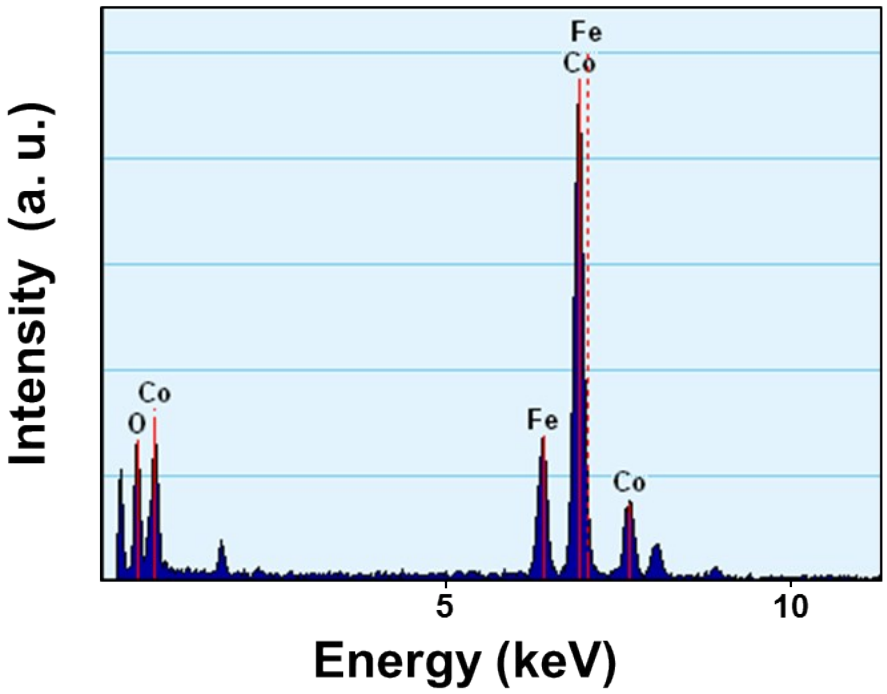

Fig. S3 EDX spectrum of the 3DOM CFO@140.

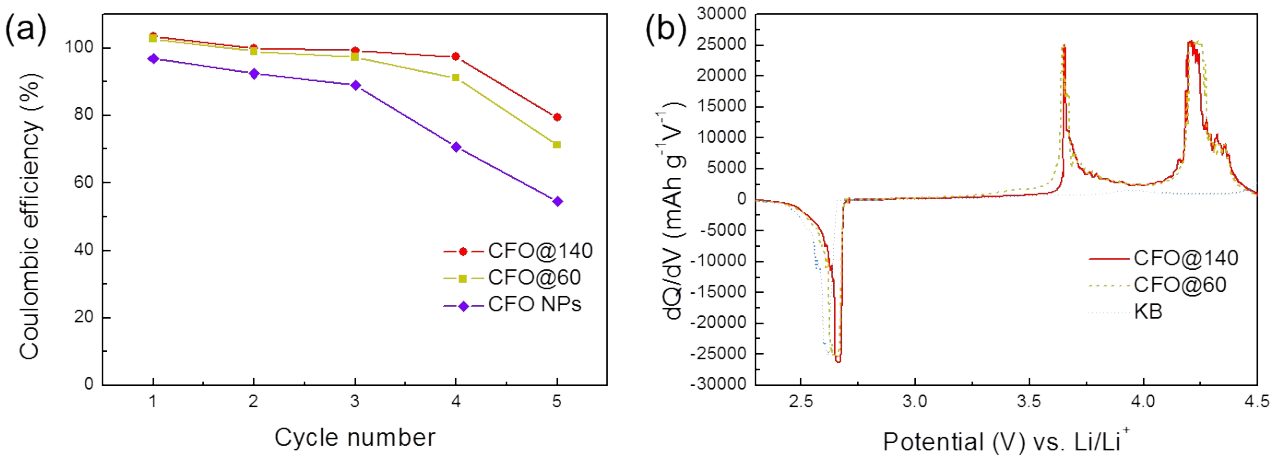

Fig. S4 (a) Coulombic efficiency-cycle number curves for Li-O_2 cells with CFO NPs, 3DOM CFO@60, and CFO@140 catalysts for five cycles. (b) Plots of the differential capacity *versus* the voltage at a current density of 200 mA g^{-1}.

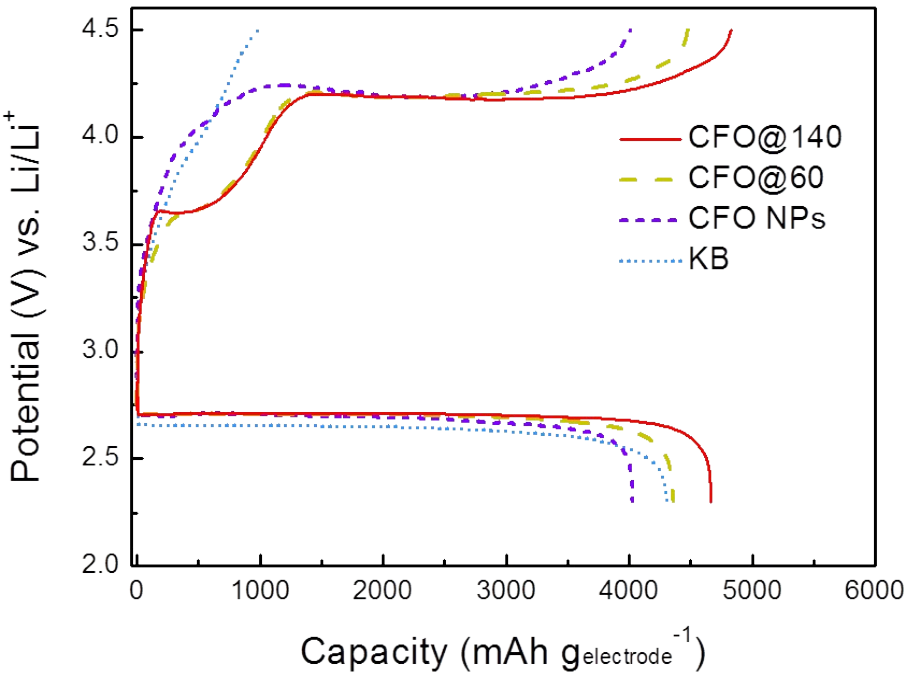

Fig. S5 The discharge-charge profiles of Li-O_2 cells with KB, CFO NPs, 3DOM CFO@60, and CFO@140 at the first cycle. The capacities are normalized by the total mass of electrode (catalyst, carbon, and binder).

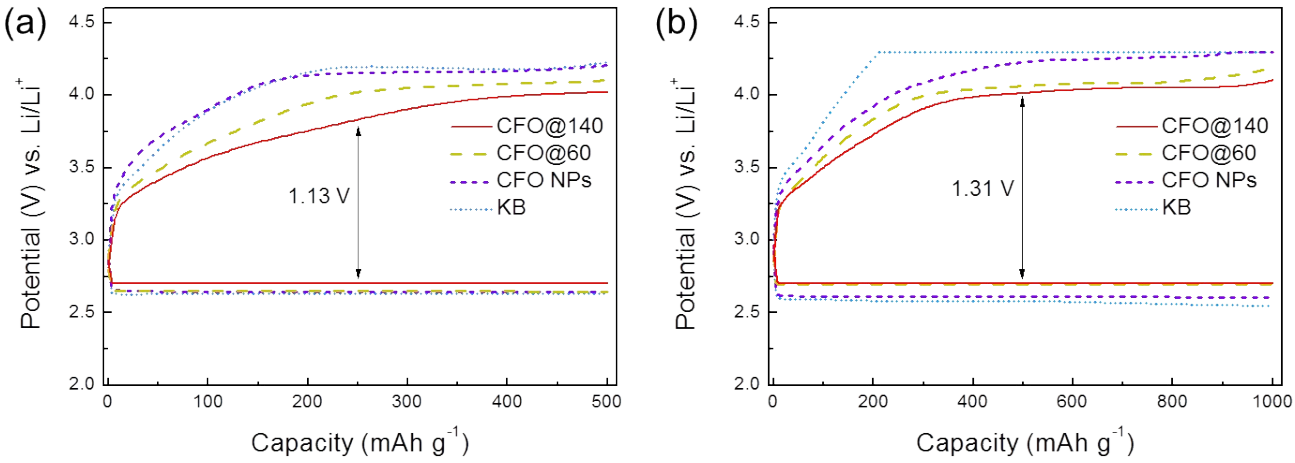

Fig. S6 Discharge-charge curves of Li-O_2 cells with KB, CFO NPs, 3DOM CFO@60, and CFO@140 catalysts at a current rate of 200 mA g^{-1} with the limited capacity depth of (a) 500 and (b) 1000 mAh g^{-1}. KB in Fig. S6b was studied in our previous work [5].

The potential-capacity curves of Li-O_2 cells with KB, CFO NPs, 3DOM CFO@60, and CFO@140 catalysts at a current density of 200 mA g^{-1} with the restricted capacity of 1000 mAh g^{-1} were provided in Fig. S6b. When increasing the restricted capacity from 500 to 1000 mAh g^{-1}, the Li-O_2 cell with CFO@140 catalyst also showed the smallest overpotential of 1.31 V as compared to that with KB (1.72 V), CFO NPs (1.62 V), CFO@60 (1.37 V). This result emphasizes again that the CFO@140 catalyst can reduce the potential polarization efficiently at a relatively high restricted capacity of 1000 mAh g^{-1}.

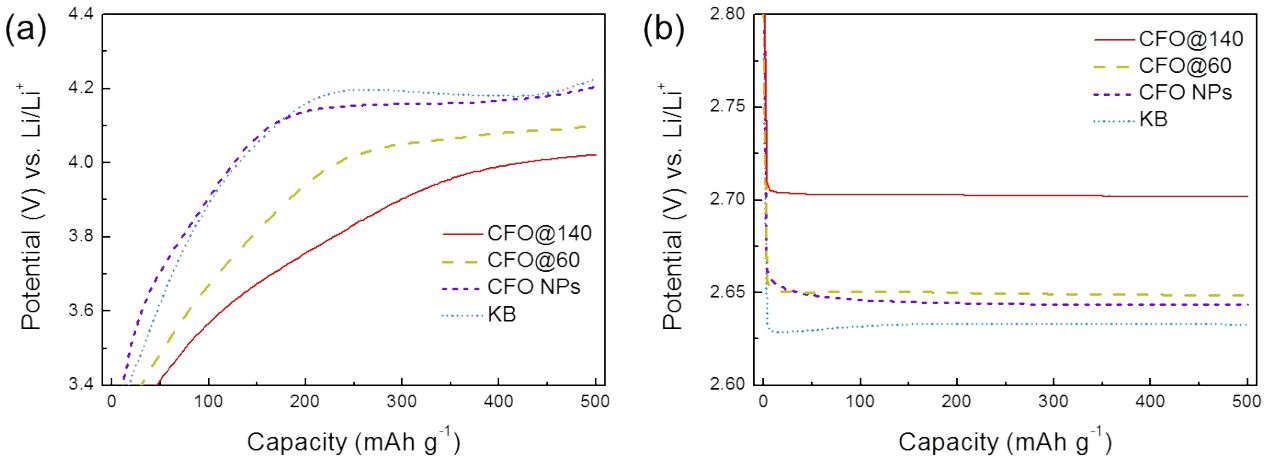

Fig. S7 Magnified potential-capacity curves for (a) initial charging and (b) initial discharging of the Li-O_2 cells with KB, CFO NPs, CFO@60, and CFO@140 at a current density of 200 mA g^{-1} with the limited capacity depth of 500 mAh g^{-1}.

For comparison of the potential polarizaion of O_2-electrode with KB, CFO NPs, CFO@60, and CFO@140 catalysts, the magnified potential-capacity profiles are provided in Fig. S7. The lowest charge potential of CFO@140 means reaction product of Li_2O_2 are decomposed more easily, while the highest discharge potential means reaction product of Li_2O_2 are formed more readily. Therefore, the CFO@140 could indicate high catalytic activity in both OER and ORR, as compared with KB, CFO NPs, and CFO@60. Consequently, the enhanced ORR/OER kinetics could lead to improvements in the energy output, the cycling stability, and the round-trip efficiency of the Li-O_2 cells.

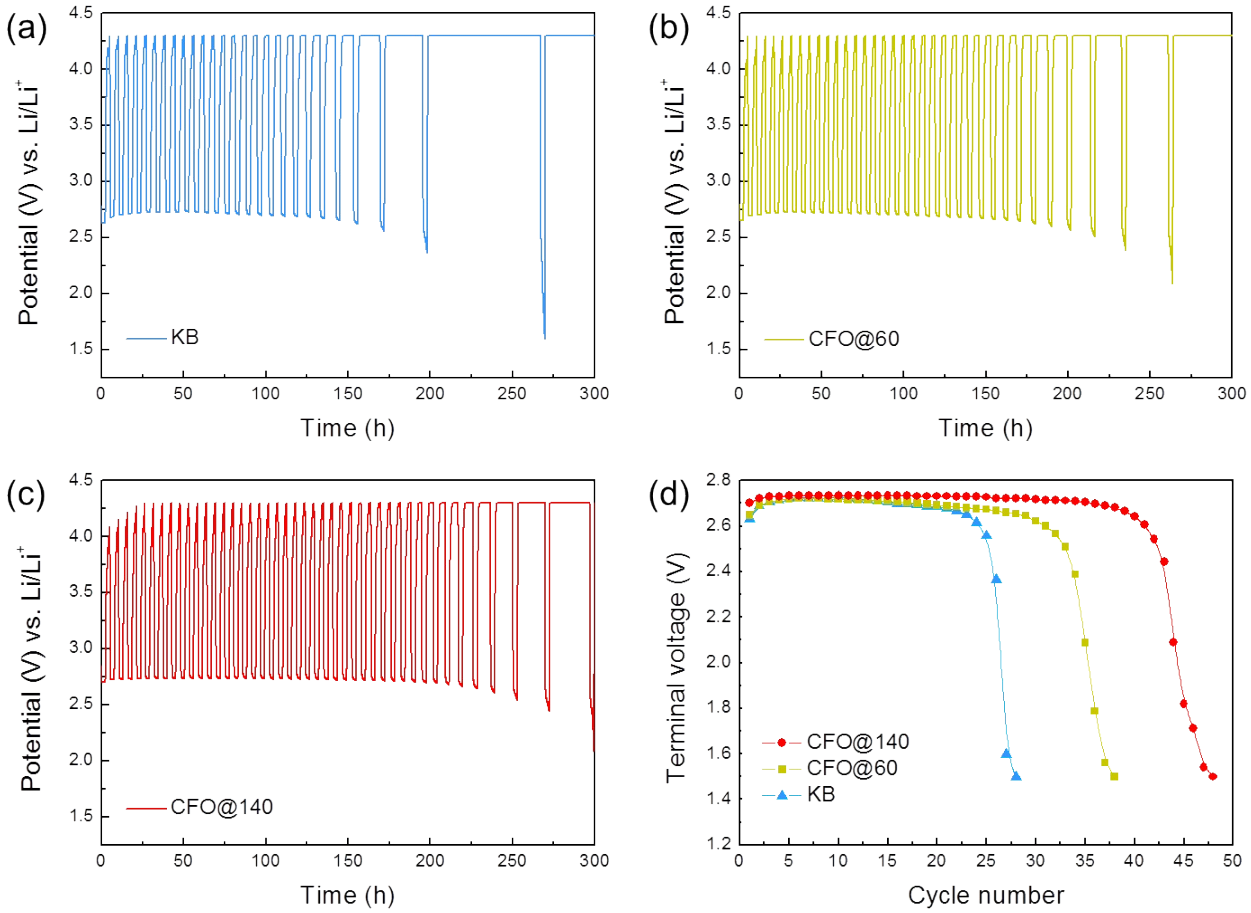

Fig. S8 Potential-time curves of Li-O_2 cells with (a) KB, (b) CFO@60, and (c) CFO@140 catalysts. (d) Terminal voltage-cycle number curves with KB, CFO@60, and CFO@140.

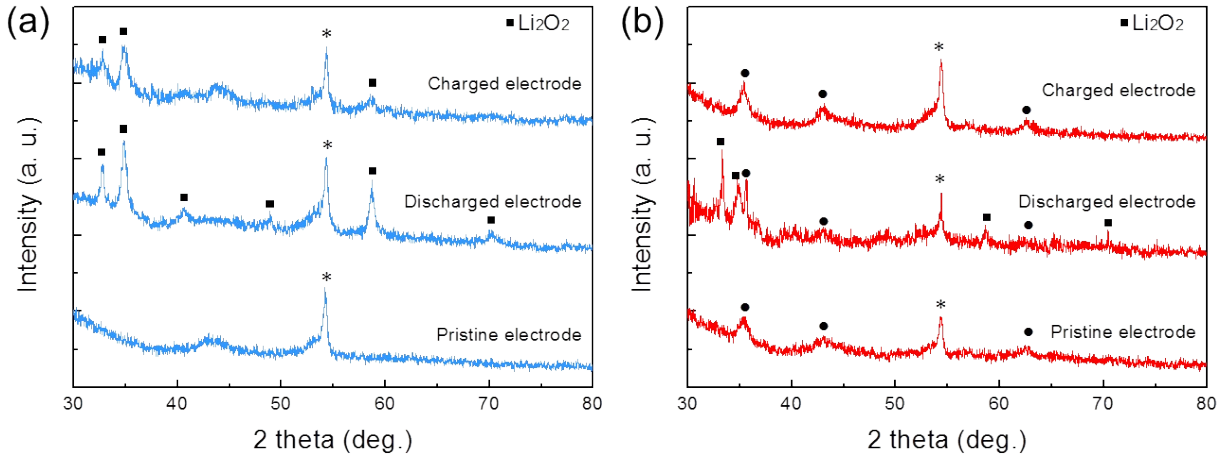

Fig. S9 XRD patterns of the O_2-electrodes with (a) KB and (b) CFO@140 at different discharge/charge stages. Peaks marked with asterisks are originated from the carbon paper.